


Trend Analysis of Total Suspended Solids in Inland Waters Using the BFAST Algorithm on MOD09GA Products in Porto Primavera Reservoir – Brazil

Análisis de tendencia del total de sólidos en suspensión en aguas interiores aplicando el algoritmo BFAST a productos MOD09GA en el embalse de Porto Primavera-Brasil

Ricardo Javier Moncayo Eraso

Universidad CESMAG, Colombia


rampa@unicesmag.edu.co

 <https://orcid.org/0000-0002-5550-6012>

Francisco Eraso-Checa

Universidad CESMAG, Colombia

feraso@unicesmag.edu.co

 <https://orcid.org/0000-0002-1432-6154>

Received: 09 January 2024

Accepted: 21 August 2024

Published: 30 August 2024



Acceso abierto diamante

Abstract

Satellite remote sensing, particularly using the MODIS orbital platform, is crucial for large-scale lake monitoring, allowing the observation of optically active components with suitable spatial and temporal resolution for lakes with surfaces greater than 40 hectares. In this context, the objective of this article was to propose a methodology that improves the retrieval and monitoring of data related to Total Suspended Solids (TSS) in large lakes. The methodology employed involved defining a baseline to map the spatiotemporal dynamics of TSS using MODIS band 1, which generates information in the infrared spectrum and is centered at 645 nm. The method was tested in the Porto Primavera Reservoir (PPR), Brazil. To validate the model, two fieldwork campaigns were conducted in the PPR, where radiometric and water quality data were collected. An empirical model was fitted between reflectance and the TSS data set ($r = 0.93$, $R^2 = 0.85$, $p < 0.01$, $n = 25$). This empirical model was applied to a time series of MODIS images from May 2000 to April 2020. Using the spatial distribution maps, a time series was created from an average pixel of the sampling stations, and then this time series was analyzed to separate the trend and seasonality. The results showed that the average TSS values observed in the time series were 5.79 mg/L. The seasonality of the time series revealed that the highest concentration is recorded in the austral summer (December-February), the rainiest season. The trend component indicates that variations in TSS concentration coincide with exceptional events of increased precipitation and with a homogenization interval of the waters following the reservoir's construction.

Keywords: BFAST algorithm, surface reflectance, temporal series, remote sensing, optical active components.

Resumen

La teledetección satelital es crucial para monitorear lagos a gran escala, permitiendo la observación de componentes ópticamente activos con una resolución espacial y temporal adecuada para lagos con superficies mayores a 40 hectáreas. El objetivo de este artículo fue proponer una metodología que mejore la recuperación y el monitoreo de los datos correspondientes a los Sólidos en Suspensión Totales (SST) en lagos de grandes dimensiones. La metodología empleada consistió en definir una línea base en la que se puede

mapear la dinámica espacio temporal de los SST a partir de la banda 1 de MODIS que genera información en el espectro infrarrojo y está centrada en los 645 nm. El método fue probado en el Embalse de Porto Primavera (EPP), Brasil. Para comprobar la validez del modelo se realizaron dos trabajos de campo en el EPP, en los que se recolectaron datos radiométricos y de calidad del agua. Un modelo empírico fue ajustado entre la reflectancia y el conjunto de datos de SST ($r = 0.93$, $R^2 = 0.85$, $p < 0.01$, $n = 25$). Este modelo empírico fue aplicado a una serie temporal de imágenes MODIS desde mayo de 2000 hasta abril de 2020. Usando los mapas de distribución espacial, se creó una serie del tiempo a partir de un píxel promedio de las estaciones de muestreo, esto se analizó para separar la tendencia y la estacionalidad. Los resultados mostraron que los valores promedio de SST observados en la serie temporal son de 5.79 mg/L. La estacionalidad de las series temporales reveló que la mayor concentración se registra en el verano austral (diciembre-febrero), la estación más lluviosa. La componente de tendencia indica que las variaciones en la concentración de SST coinciden con eventos excepcionales de aumento de precipitaciones y con un intervalo de homogeneización de las aguas posterior a la construcción del embalse.

Palabras clave: Algoritmo BFAST, reflectancia de superficie, series temporales, teledetección, variable ópticamente activa.

Highlights

BFAST is a remote sensing tool that allows the observation of optically active components of the waters.

BFAST models the trend of the variable, highlighting the differences between the observed and modeled values.

The BFAST algorithm for MOD09GA products considers interannual variability.

Highlights

BFAST es una herramienta para la teledetección que permite la observación de componentes ópticamente activos de las aguas.

BFAST modela la tendencia de las variables, resaltando las diferencias entre los valores observados y los modelados.

El algoritmo BFAST en productos MOD09GA considera la variabilidad interanual.

1. INTRODUCTION

Continental and coastal waterbodies are considered highly sensitive strategic ecosystems to anthropogenic pressure and climate change [1], [2]. It is important to consider that around these natural environments is concentrated more than 60 % of the world's population [3]. Besides, people use the water in activities such as fishing, human consumption, agriculture, industry, recreation, tourism, and electricity generation. These multiple uses of the water can cause several environmental problems that might have a direct impact on its quality [4].

According to [3], [5]-[7] one of the main indicators that determines how healthy an aquatic ecosystem is, is the clarity (turbidity), which is influenced by the amount of dissolved matter and TSS. These particles can vary in size and range from nanoscale to sand-sized sediments. An excess of suspended solids can cause a lot of detrimental effects on water resources, causing problems such as decreased light availability for primary productivity, eutrophication, hypoxia, and algae proliferation in the aquatic environment [2], [8]-[11].

Consequently, authors such as [12], [13] indicate that monitoring the TSS variable constantly in an aquatic environment is indispensable, taking into account the high diversity and dynamics in the spatial and temporal domains of this parameter in continental waterbodies. In this context, [14]-[16] show that traditional in situ sampling techniques are limited when it looks for representing the spatial and temporal variability of a waterbody. Thus, it is recommended the use of remote sensing methodologies to have a synoptic view of the lake and obtain an estimated measurement with a high time frequency of the variable of interest.

Thus, models to calculate TSS concentration can use a single-band empirical algorithm, or something that involves performing a previous band mathematical process, where the reflectance captured by the remote sensor is directly related to TSS measurements collected in situ [3], [17], [18]. To achieve the correlation model, statistical techniques are used, which can be linear or nonlinear. According to [9], [19], [20] the most suitable regions that have electromagnetic spectrum to estimate TSS concentration are located in the red and near-infrared spectral bands. According to [21]-[24] they demonstrate that the remote estimation models used may have a coefficient of determination greater than 0.7, provided that TSS concentrations vary between 5 mg. L⁻¹ to 200 mg. L⁻¹.

In accordance with [3], [8], [17], [25] IKONOS, MERIS (MEdium Resolution Imaging Spectrometer), SPOT (Satellite Pour l'Observation de la Terre), Landsat and MODIS (Moderate Resolution Imaging Spectroradiometer) sensors possess spectral bands which are carefully positioned to estimate the concentration

of TSS in water. Of the above mentioned sensors, MODIS has presented the best results. Authors such as [18], [19], [24], [26] claim that the reasons for this positive performance, is that MODIS has a higher spectral resolution (36-band, 8-band in its spectral range of red and infrared light) [27], it generates a daily surface reflectance product (MOD09GA) and their average spatial resolution (250 m, 500 m and 1000 m) allow large bodies of water (greater than 40 Ha) to be mapped in a single frame [28], [29].

Based on the aforementioned ideas, it is defined that monitoring optically active variables using medium-resolution images with high temporal frequency can be performed in a large lake like the PPR [28], [29]. This reservoir is located among the states of São Paulo, Mato Grosso do Sul, and Paraná, it includes several water bodies, and is situated in the Paraná River floodplain. The region's climate is humid subtropical mesothermal, with a drier period from June to August [30], [31]. The construction of the Porto Primavera dam caused significant socio-environmental changes, flooding 80 % of the area on the Mato Grosso side [32]. The reservoir extends from the Jupuí dam to Primavera in São Paulo. This development affected over 50 % of the floodplain between the Jupuí and Itaipú dams, disrupting ecological, economic, and cultural activities [31], [32].

The primary objective of this research was to generate a time series with a homogeneous frequency (1 month) using MODIS images, which are suitable for monitoring the flooded area in the Porto Primavera Reservoir and analyzing optically active limnological variables such as TSS.

The analysis focuses on identifying the most significant changes in the TSS parameter trend over 20 years (May 2000 to April 2020) using the BFAST (Breaks for Additive Season and Trend) algorithm. BFAST is an algorithm that detects long-term trend changes in natural phenomena through statistical tests and the identification of breakpoints in time series data [33]. Its primary application in remote sensing is in phenological studies, making it a valuable tool for remote sensing studies of inland and coastal waters. BFAST models the variable's trend, highlighting the differences between observed and modeled values, and considers interannual variability [34], [35]. To work effectively, BFAST relies on historical data to generate a baseline model and detect interannual alterations over the monitoring period. This R library can detect both gradual and abrupt changes, including multiple breakpoints and seasonal variations. In this study, BFAST was employed to characterize the timing, magnitude, and direction of changes, identifying disturbance events in the TSS variable. This approach enables the analysis of the impacts of abrupt climatic changes or natural lake dynamics on the TSS over 20 years, highlighting periods of significant increase or decrease.

2. MATERIALS AND METHODS

2.1 Geographic location

The Porto Primavera reservoir (53° W to 52° W and 22° S to 22° S -30° S), as shown in Figure 1a, is located in the south-west of Brazil [32]. The maximum depth of the lake is 35 m and occupies an area of 2500 km. [31]. The wall built to form the reservoir, is the largest in the country, with a length of 10186.20 m. The main function of this reservoir is the generation of electricity, with a capacity of 1814 MW, which corresponds to 23 % of the energy consumed by the State of Sao Paulo [36], [37].



Figure 1.

Geographical location of the Porto Primavera reservoir. (a) The water basin of the reservoir is indicated in the circle. (b) Displays reservoir boundaries and spatial distribution of sampling points. The dotted areas (circles) indicate 1) mouth of the Rio do Peixe; 2) Pardo River mouth; 3) Transition zone; 4) region near the reservoir wall.

Source: own elaboration.

2.2 Methodology

Five main processes were conducted in order to extract the historical concentration of TSS variable over a period of 20 years using MODIS images (MOD09GA) in PPR (Figure 2). The process (a) shows field campaigns radiometric and TSS data collection in PPR, next step (b) was download the MODIS images and clip spatial and spectrally MOD09GA products. Quality Control bands (state_1 km and QC_500 m) that come with the MOD09GA reflectance products are used to ensure the quality of the images, the resulting image is converted to surface reflectance (box c). The TSS values obtained in the laboratory are correlated, analytically, with the field spectral data corresponding to the band centered at 645 nm, the model is extrapolated to a time series of 252 MODIS images (box d). Finally, time series vectors are extracted from pixels that match the sampling points, an average vector is obtained from the 25 sampling observations, and lastly the average time series is separated and analyzed using the BFAST algorithm (box e).

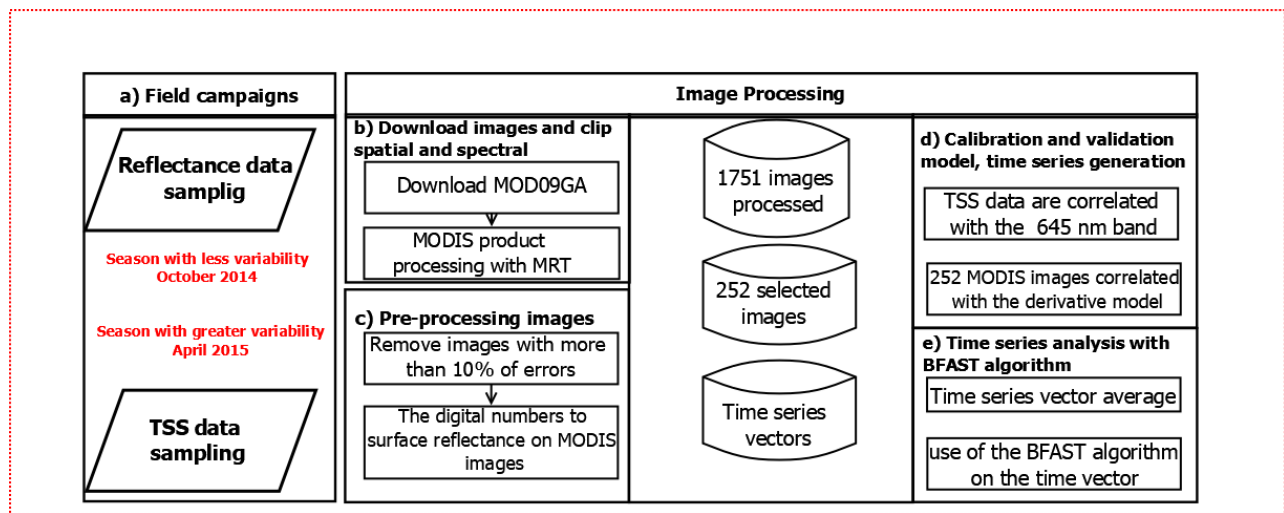


Figure 2.

Flow-chart of the methodology applied in this study.

Source: own elaboration.

2.2.1 Data collection

Figure 1b illustrates the spatial distribution of 25 sampling points located throughout the PPR. To determine the optimal locations for these sampling stations and the best times for sampling campaigns, a time series of MODIS images from May 2000 to April 2013 (156 scenes at one-month intervals) was used. These images were preprocessed as described in Chapter 2.2.3. The R1MODIS (645 nm) was applied to determine TSS concentration, allowing for the identification of sampling points with the highest variability over the 13-year period, given the strong correlation between this band and TSS concentration in tropical waters [38] (Figure 3).

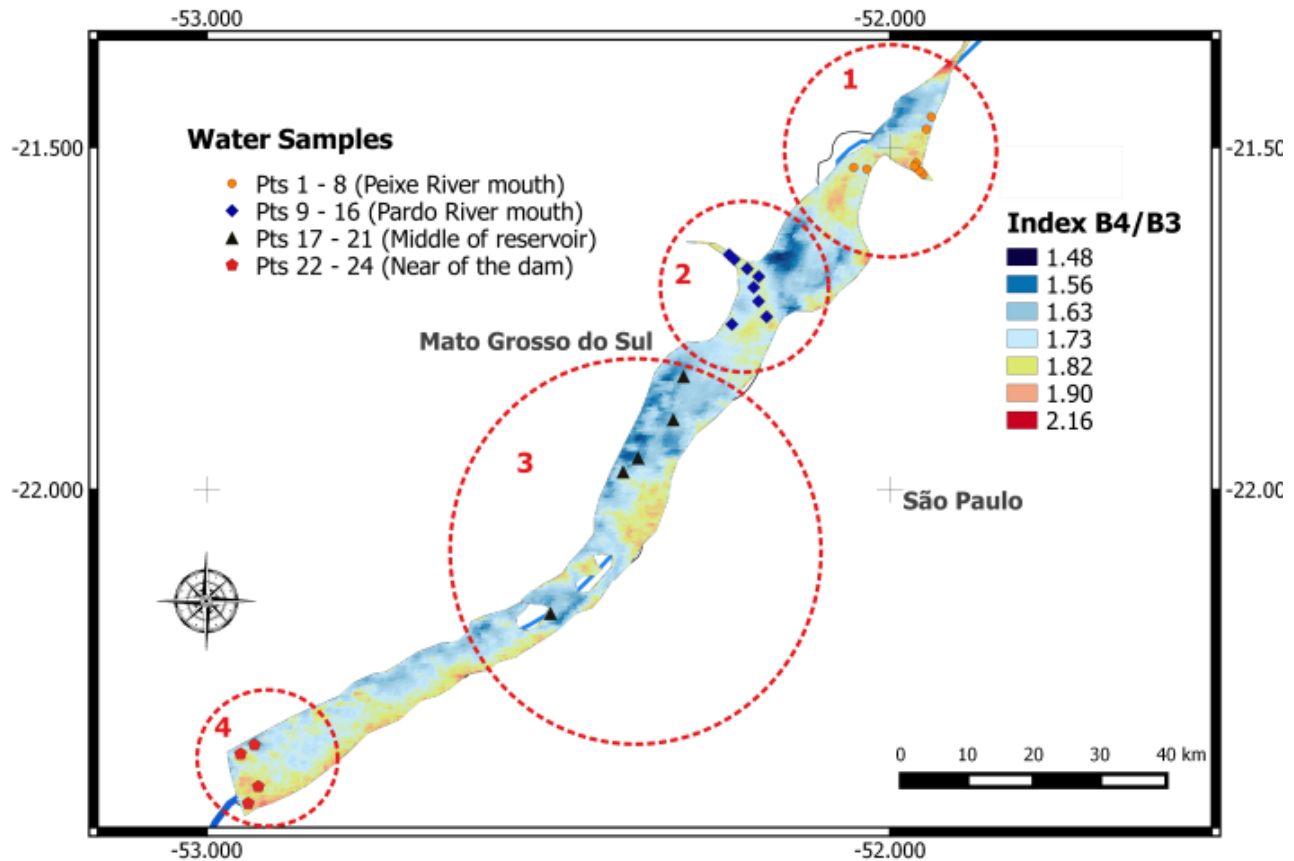


Figure 3.

Map of temporal average standard deviation intervals of bands ratio B4/B3 and the distribution of sampling units.

Dashed lines show the sampling point groups in PPR.

Source: own elaboration.

To determine the most suitable seasons for sampling, the same set of images was used to create monthly average images. The average value of each image was analyzed to identify the seasons with the highest (fall) and lowest (spring) variability in TSS concentrations. This analysis indicated that autumn and spring were the most appropriate seasons for conducting sampling campaigns in the reservoir.

Fieldwork was applied on dates when the TSS parameter had less (October 6th ~ 10th (2014) and greater variability (April 13th ~ 16th (2015)). The data include a total of 49 samples, 24 samples from October (2014) and 25 samples from April (2015). Table 1 shows the exploratory analysis data and descriptive statistics of TSS in field campaigns. The collection of spectroradiometry samples were carried out between 9 am and 3 pm local time. In order to measure and analyze the TSS variable, it was necessary to collect water samples in bottles and filter their contents using a vacuum pump and Whatman filters of 0.5 μm –0.7 μm . These filters were previously incinerated at 480 .C for six hours in a muffle and weighed on an analytical balance before being released to fieldwork. Once in situ sampling was completed, the filters were stored at -4.C in a refrigerator and then dried for 24 hours at 60.C on a stove. At the end, the filters were weighed again and (1) was used to determine the total amount of matter suspended in water [39].

Table 1
Summary of TTS concentration N49 in fieldworks of October 2014 and April 2015

Date	Samples			TSS Concentration mg•L-1			
	Total	Calibration	Validation	Max	Min	Mean	Standard des
October 2014	25	24		14.78	0.2	4.06	4.58
April 2015	25		24	18.15	0.019	5.5	5.57

Source: own elaboration.

$$TSS \frac{mg}{L} = \frac{(A - B) * 1000}{C} \quad (1)$$

Where, A: filter weight after filtering water contained in the bottles; B: filter weight before being released to field work; C: volume of filtered water.

2.2.2 MODIS product and digital image processing

The MODIS sensor, which is aboard the Terra orbital platform, has been taking images of the earth since 2000. The products obtained by this sensor have between 2 to 36 spectral bands, and their values can be expressed in radiance scaling or surface reflectance [8], [15], [40], [41]. One of the products generated by the sensor is MOD09GA; this contains surface reflectance data that is generated on a daily basis and a spatial resolution of 500 m [28].

For this study, MODIS images were downloaded from the United States Geological Survey (USGS) (<http://earthexplorer.usgs.gov/>) website, and a total of 1751 images were taken from May 2000 to April 2020. According to [17], [27], [42], the bands located at the spectral intervals of red and infrared provide sufficient sensitivity to correlate their reflectance values with water quality indicators such as TSS. For this particular study, band 1 (620 nm -670 nm) was used, which it was possible to recover the concentration of TSS in the Porto Primavera reservoir.

2.2.3 Image processing

To generate the time series of MOD09GA products between May 2000 and April 2020 month by month, a total of 1751 images were downloaded. Subsequently, these images were pre-processed by performing the following actions: spectral trimming, spatial trimming, UTM mapping re-projection, and pixel resampling at 250 m using the nearest neighbor interpolation method and the MODIS Reprojection Tools (MRT). When using the equation defined by [43] (2), the values of the digital numbers contained in the reflectance image were converted. To make all processes faster, it was necessary to create computational routines in the Python and R languages to perform parallel tasks. Using routines developed in the Python programming language, .prm files necessary for performing spatial and spectral cropping of MODIS images are created. Subsequently, using the pyhdf.SD library available in Python version 2.7, the elements contained in the HDF meta-file are processed.

$$\frac{P_i}{10000} \quad (2)$$

Where is the pixel at the i position of any of the reflectance bands contained in the MOD09GA product.

The next step was to use the quality assessment bands State_1km_1, QC_500m_1 to determine the pixel quality of the image; this process allowed to eliminate images that had more than 10 % errors by cloud occlusion or sensor errors. After the sub-pixel debugging process was completed, the images with fewer errors were chosen for a month. The Python computational routine in this step allowed for the evaluation of each pixel and the creation of a new, error-free file that can be detected during the production of MODIS products. As a result, a time series was obtained with 252 observations. To achieve a time series with a homogeneous frequency, it was necessary to use interpolation techniques such as moving average, to create an average image in the months when it was not possible to have one image at least with less than 10 % error.

2.2.4 Spectral analysis

Water surface reflectance measurements were performed using a FieldSpec UV/VNIR ASD HandHeld spectroradiometer, which has a spectral resolution of 355 nm to 1075 nm and a sample range of 1.6 nm. The signal collected by the computer is quantified in 16 bits [44]. In this work, the Hemispherical-Conical Reflectance Factor (HCRF) was measured, as shown in the reflectance curves analyzed in (Figure 2). Then, in order to obtain surface reflectance measurements, it was collected spectroradiometry readings from the waterbody, sky, and spectralon reference panel for each point. Equation (3) defined by [45] is used to obtain the surface reflectance curve.

$$R_{rs} = \frac{(L_t - \rho L_s)}{\left(\frac{\pi}{R_g} L_g\right)} \quad (3)$$

Therefore: L_t is the total radiance captured by the spectroradiometer coming from the waterbody; ρ is the radiation that comes from the sky (skylight) in the air-water interface which depends on the azimuth, data acquisition geometry, wind speed and surface roughness; L_s is diffuse sky radiation and has no information about water; R_g is about fiducial marker reflectance measured under controlled conditions (laboratory); L_g is the radiance measured in the field of view.

2.2.5 Integrating MODIS spectral bands

Before creating the empirical model estimation for the TSS variable in the region, it was necessary to convert the measured field reflectance, using the response functions for band 1 in the MODIS sensor. This process was carried out in order to simulate the remote sensing reflectance signals ($R_{rs}(\lambda_i)$) recorded by the sensor and centered on a given λ_i wavelength. Equation (4) allows to obtain the reflectance data of each MODIS spectral band [46], [47].

$$R_{rs}(Bi) = \frac{\sum_{\lambda_1}^{\lambda_n} S(\lambda) R_{rs}(\lambda)}{\sum_{\lambda_1}^{\lambda_n} S(\lambda)} \quad (4)$$

Where λ_1 and λ_n are the lower and upper limits of the band (Bi being $i = 1, 2, \dots, 36$). $S(\lambda)$ is the spectral response function [48]. $R_{rs}(\lambda)$ signal collected in the field with the FieldSpec UV/VNIR ASD HandHeld spectroradiometer.

2.2.6 Empirical regional model and estimating measurement uncertainty associated with the model

A large number of regional algorithms have been developed to estimate the TSS variable; these can be calculated from the correlation between the concentration of the variable measured in-situ and the reflectance

contained in the image pixels and using the measure field reflectance collected (the models found among the relationships of the variables can be linear, quadratic, exponential, logarithmic or polynomial type) [49], [9].

According to [3], [40], empirical estimation algorithms using band 1 (B1 645 nm) and band 2 (B2 858.5 nm) of MODIS sensor can be classified into six categories: with a single band (B1, B2), difference between two bands (B1-B2), sediment index $((B1-B2)/(B1+B2))$, band division (B2/B1) and division logarithm $(\log(Rrs(B2)) / (\log(Rrs(B1))))$.

As stated above and according to [50]-[54], the best wavelength to recover TSS values lower than 200 mg L⁻¹ is located in the red light spectral intervals (620 nm to 670 nm). Therefore, it is defined that to estimate the TSS in the PPR, it is possible use a single band algorithm that uses the spectral channel centered at 645 nm (B1), the above, taking into consideration that the body of water does not present readings greater than 30 mgL⁻¹. Once the MODIS band is selected, we proceeded to correlate the pixel reflectance of the MODIS image, and the field read with the TSS concentration. With the two field campaigns conducted on the lake, a dataset is separated to calibrate the model (samples collected in October 2014) and validate it (samples collected in April 2015).

In order to validate the applicability of the model to estimate the TSS, the statistical estimators R2, MAE (5), MSE (6), RMSE (7), %RMSE (8) and p-value were used.

$$MAE = \frac{1}{N} \sum_{i=1}^N |X_{esti,i} - X_{med,i}| \quad (5)$$

$$MSE = \frac{\sum_{i=1}^N (X_{esti,i} - X_{med,i})^2}{N} \quad (6)$$

$$RMSE = \sqrt{\frac{\sum_{i=1}^n (X_{esti} - X_{med})^2}{N}} \quad (7)$$

$$(\%) RMSE = \frac{RMSE}{MAXX_{med} - MINX_{med}} \quad (8)$$

In the previous equations, Xesti is the value of the TSS parameter estimated by the empirical algorithm. Xmed is the TSS value measured in the lab. MAX and MIN are the maximum and minimum TSS values read in the lab.

2.2.7 Generation and analysis of the TSS parameter time series

To extrapolate the empirical algorithm in October 2014 field campaign (calibration model) into the 252 MODIS images in the time series, the procedure defined by [55] is followed. Subsequently, temporary vectors are extracted from the 25 sampling stations and an average temporal vector of these observations is generated. From the time series, the trend and seasonality components are extracted to be analyzed using the R Breaks For Additive Seasonal and Trends (BFAST) language library [56], [57].

The main improvement that BFAST presents over other temporary decomposition libraries, such as decompose and Seasonal and Trend decomposition using Loess STL, it is that allows to characterize the intervals (date, sign and magnitude) where gradual and abrupt changes occur that affect the magnitude and trend direction [58], [59].

3. RESULTS AND DISCUSSION

3.1 Results

3.1.1 Spectral data analysis

Once the spectral curves generated by the field spectroradiometer were obtained, a classification is carried out to discriminate the areas where the hyperspectral samples were collected and the dates on which the fieldwork was performed (Figure 2). It is observed in the graphs that all spectral curves show a characteristic behavior of water, there is a low reflectance in the spectral range from 400 nm to 500 nm associated with strong absorption by organic matter.

The spectral curves obtained at some sampling stations maintained similar characteristics in two fieldworks. The points collected at the mouth of the Peixe River (2A), transition zone (2C) and in the regions near the barrier, showed that the spectral curves are similar to those published by [17], [60]-[64] especially with bodies of water with a dominant presence of Chl-a. However, the estimated concentrations of Chl-a in the Porto Primavera reservoir are lower than those found by the aforementioned authors.

The set of spectral curves measured in the Pardo River, have a flat shape between 570 nm and 670 nm, which according to [17], [44], [64] can be associated with high content of suspended solids in the water.

3.1.2 Calibration and validation models

In order to test and validate the performance of the TSS empirical recovery algorithm, calibration and validation models are created to verify the accuracy between relationships: TSS concentration – field measurement of reflectance. Table 1 shows some statistical aspects of the measurements carried out in-situ for the TSS, it can be verified that for the two field works the results are very similar, increasing in some statistical values (average, maximum, standard deviation) in the fieldwork carried out in the austral fall (April 2015). Taking into account the statistical characteristics of the TSS data sets, it is defined that to find the calibration model (Figure 3) the fieldwork dataset collected in October 2014 (n. 24) was used. The results indicate that the quadratic function (9) showed a better fit in its coefficient of determination ($R^2 = 0.859$). According to [3], [7], [49], estimation models with an $R^2 > 0.7$, can be considered suitable to estimate the TSS variable in both inland and coastal waters.

$$TSS_{mgL^{-1}} = 23218 * (Rrs(B_1))^2 - (187,8 * (Rrs(B_1))) + 1,085 \quad (9)$$

The fieldwork carried out in April 2015 was used to validate the model (Figure 4). The data collected in this sampling campaign confirm that the performance of the algorithm remains satisfactory to retrieve the values of the TSS variable ($R^2 = 0.82$; RMSE 2.74). The results coming from the statistical estimators indicate that the model used (Figure 5) shows an adequate degree of accuracy and consistency in predictive results (Figure 6).

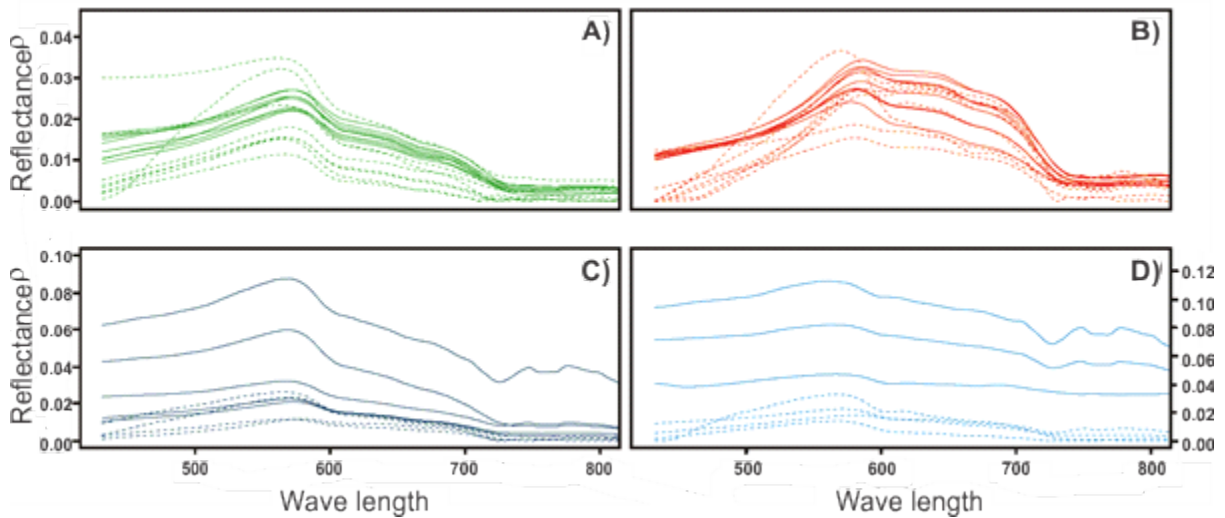


Figure 4.

Reflectance curves taken at the sample points located in. (a) Rio do Peixe river mouth; (b) Rio Pardo river mouth; (c) Transition zone; (d) Region near the wall.

Source: own elaboration.

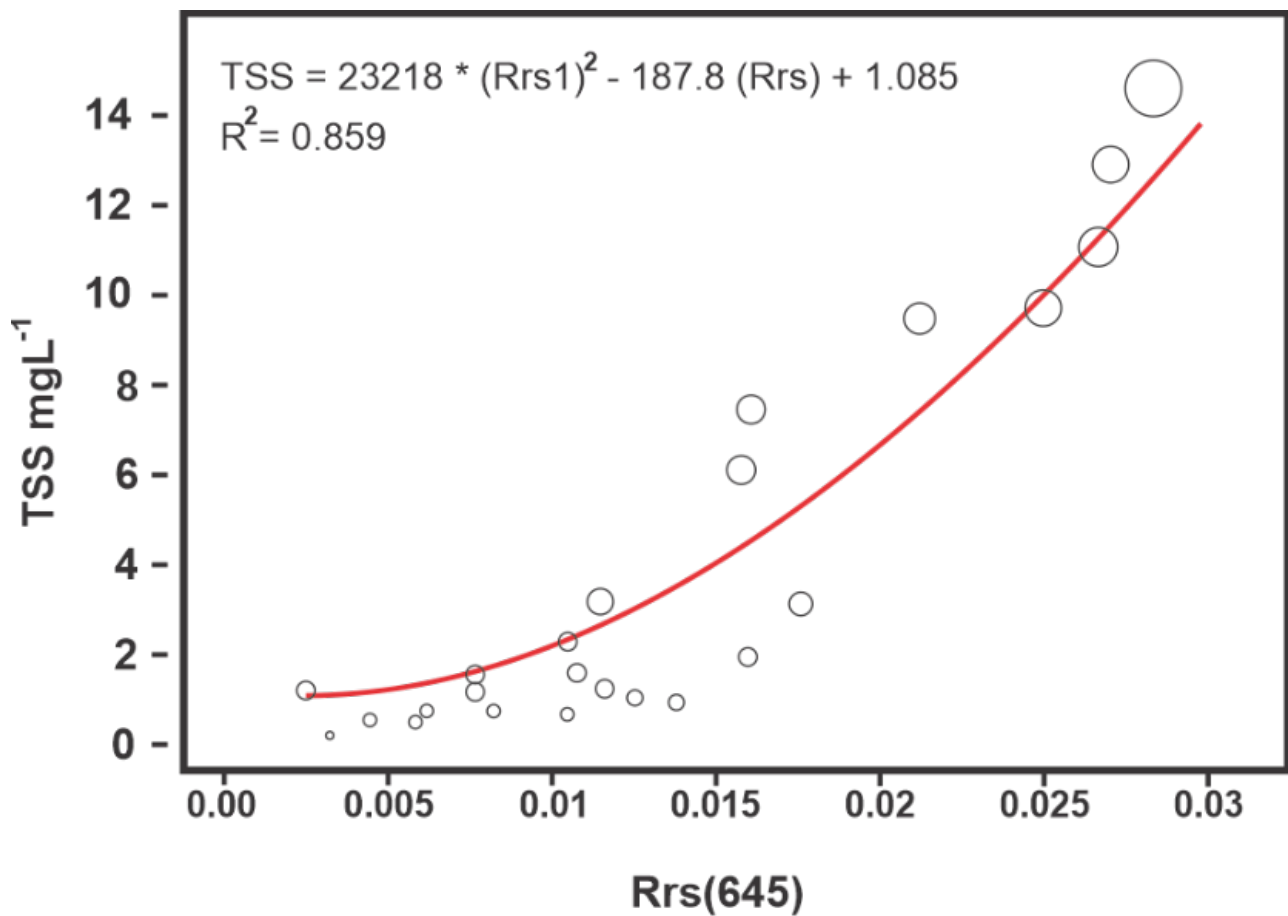


Figure 5.

Calibration model for the TSS variable. The correlation model considered the measured field reflectance for band 1 of the MOD09GA product and the TSS concentration measured in October 2014 at 23 sampling points.

Source: own elaboration.

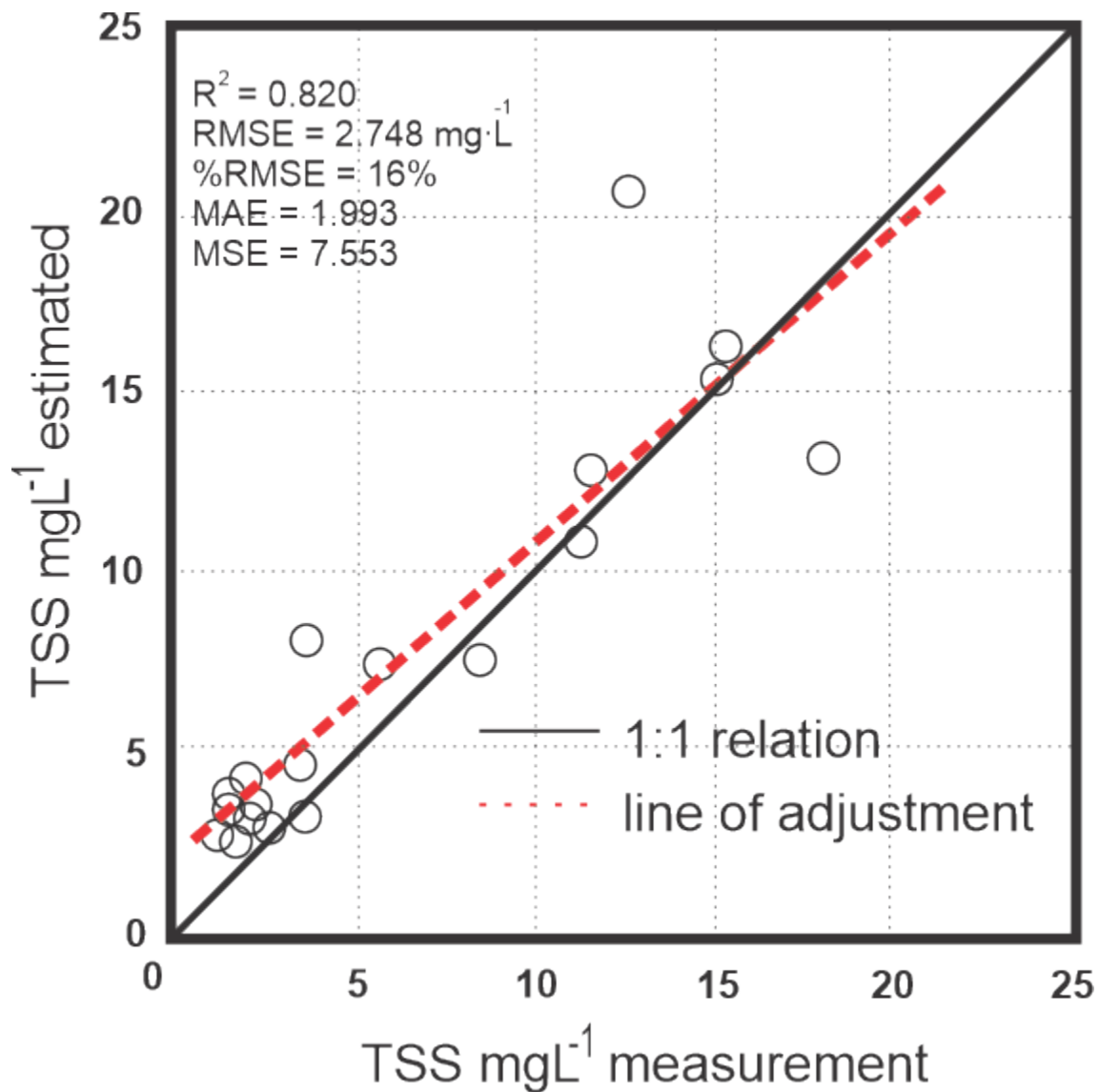


Figure 6.

Model validation for the recovery of the TSS variable, performed from the spectroradiometry and TSS concentration data, taken in April 2015.

Source: own elaboration.

3.1.3 Analysis of the time series components in the TSS parameter

Description of the variation points in the time series trend

Figure 7 shows the variability of the average time series extracted from the pixels of the MODIS images for the 25 sampling points. The graph reflects the variations on trend component in the period 2000 to 2020 as well as the periods in which break points occur due to changes in the magnitude and frequency of the TSS values.

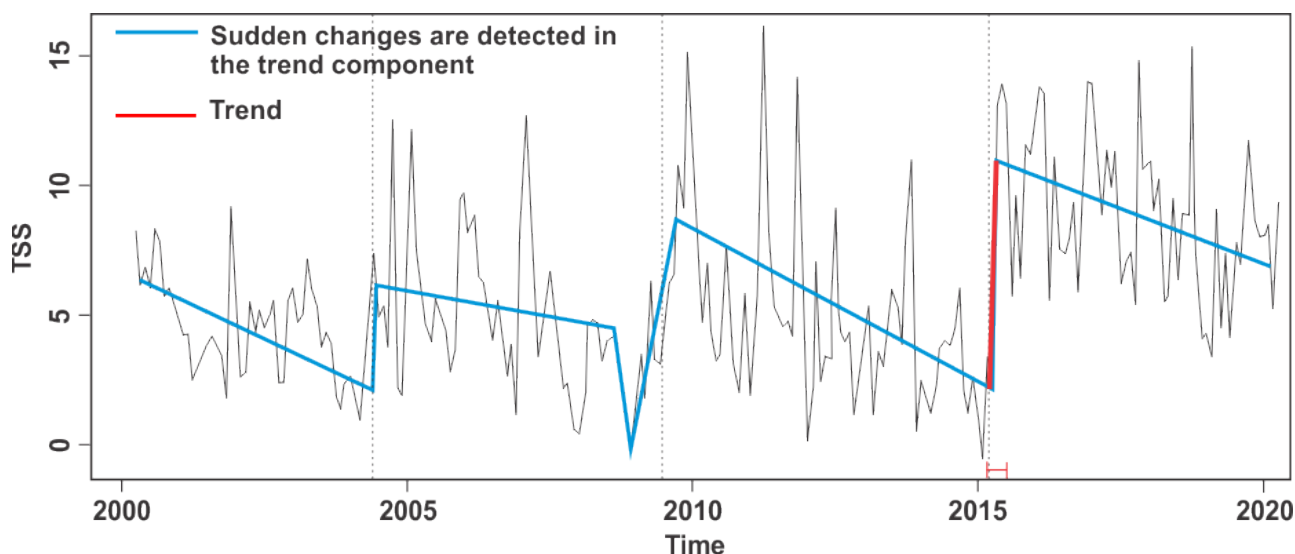


Figure 7.

Change points in the time series trend of the TSS variable in the Porto Primavera reservoir from May 2000 to April 2020.

Source: own elaboration.

To [59], [65], the break points analysis on trend component is realized by researchers to know possible reasons that originated them. In this respect, the analysis done for each of the periods that show break points in the TSS temporal series of PPR, have indicated that four intervals registered a gradual increase in the TSS concentrations in the reservoir, however, exceptional climatic events have altered the periodicity and intensity of factors (rains) that directly affect the TSS, permanently affecting the concentration of this parameter in the lake.

Within the first two periods (A and B), the trend of the TSS parameter was stable with a slight increase in period B, for the interval 2000 to 2009, two fundamental aspects that affect the result can be considered, the first of them is the construction of the reservoir, where at the beginning of the flood (1998-2001) the amount of material in suspension in the lake registered values higher than 5 mgL⁻¹. Nevertheless, the lake waters began to gradually homogenize the TSS content, this factor being accelerated by the size (2250 km.) and average depth (30 mts) of the lake [66], which is reflected in a progressive decrease in the parameter. The second important aspect of this period is that the oscillations in the variable depend on the dry (autumn-winter) and rainy (spring-summer) seasons.

The second interval of interest on trend analysis is the breaking point that begins in the spring of 2009 and that extends until the fall of 2015, this interval shows an exceptional change that alters the dynamics of the TSS in PPR, this change is due to the climatic phenomenon known as "la Niña" which increased the frequency and quantity of rains in the region in the period 2010 to 2011. This precipitation anomaly result in a large amount of particulate material in the waters of the reservoir produced by the tributaries and the runoff from the crops surrounding the lake, due to this increase in the rains, TSS concentration almost doubled in a relatively short period of time (4.93 mgL⁻¹ 2000-2009 to 8.83 mgL⁻¹ 2009 to 2011). For the last period (2015-2020), the reservoir has not been able to reestablish the values prior to 2009, on the contrary, they have increased obtaining an average value of 8.96 mgL⁻¹.

Analysis of TSS seasonality in Porto Primavera Lake

In order to understand the TSS seasonality in the water body, Figure 8 is generated; this graph indicates that there is a regularity and coincidence with the driest and rainiest seasons of the year, the highest concentration of suspended solids occurs in the spring-autumn interval (October-April), this season corresponds to the months where there is the greatest precipitation in the region (October-February), and subsequently there is a

growth of algae in the lake that affects transparency in the water column (March-April). The decrease in TSS concentrations corresponds to the driest and coldest season of the year, where temperature shortens algae growth, and low rainfall limits the flow of particulate matter from the cultivated margins around the lake.

To complement the findings of Figure 8, Table 2 shows a descriptive statistical analysis of the seasonality found in the TSS concentration time series, it was detected that the maximum value within the entire time series was presented in the month of May (autumn) 2011, the lowest value was presented in October 2009, the highest average values occurs in the summer season, a season that coincides with the highest amount of rainfall in southern latitudes. In the same way, it is found from the data in this table that the average increase in TSS in the winter-spring seasons is 0.94 mgL⁻¹ and in the change of spring-summer season it is on average 3.49 mgL⁻¹, this increase is due to the greater occurrence of rains, which generate a large amount of particulate material that ends up in the reservoir.

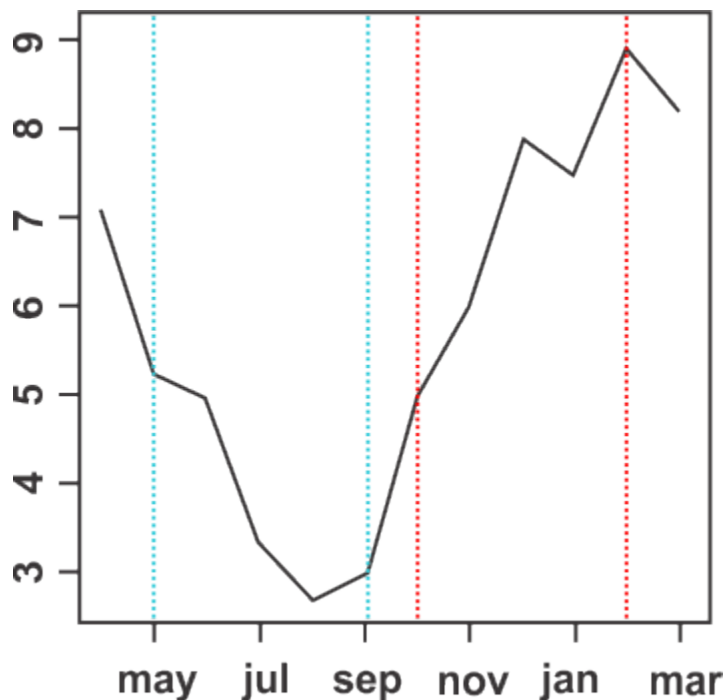


Figure 8.

Seasonality presented in the TSS variable in Porto Primavera Lake. The blue lines indicate the months with the least number of suspended solids. The red lines show the months in which TSS present the highest concentrations.

Source: own elaboration.

Table 2

Statistics of TSS in Porto Primavera Reservoir during 2000 to 2020

Statistics	Seasons			
	Spring	Summer	Fall	Winter
Max	15.04	17.29	17.41	13.12
Min	0.90	1.53	2.42	0.98
Average	4.60	8.09	6.89	3.66
Standard deviation	3.92	4.50	3.44	2.48

Source: own elaboration.

3.2 Discussion

3.2.1 Evaluation of the empirical model for TSS recovery

As well as in the researches developed by [5], [17], [58], [67], [68], in the PPR is possible to make use of the spectral region located in the wavelength of red light (620 nm-750 nm), the aforementioned authors indicate that this band of the electromagnetic spectrum has a direct relationship with the increase in the concentration of the TSS. However, they mention in their studies that at this wavelength it is possible to successfully recover values lower than 200 mgL⁻¹. Taking into account that in the in-situ work in the PPR, values higher than 25 mgL⁻¹ were not recorded, it is possible to conclude that the use of band1 (645 nm) of the MODIS sensor to derive the TSS concentration in the lake is appropriate. The results show that an algorithm based on the band embedded in 645nm is quite accurately for estimating the variable, which also has a low error associated with its estimated values.

3.2.2 Interpretation of break points in the trend of TSS concentration and its seasonality

We propose to use a novel tool that combines remote sensing and the BFAST time series analysis algorithm. This tool enables us to analyze different components of a time series and examine the magnitude of changes in the trend. The BFAST algorithm is commonly used to study changes in land cover, and its potential application in analyzing bodies of water has been relatively unexplored. Using remote sensing data allows for an evaluation directly linked to the dynamics of the TSS variable's concentration and how it may be permanently impacted by extreme weather events, as demonstrated in this study. These findings align with research on Qinghai Lake, showing a strong correlation between seasons and climatic and land cover variables, resulting in breakpoints in the time series of optically active aquatic variables [69].

After analyzing the performance and findings obtained from using BFAST in the PPR, we observed two important aspects for all the breaking points. First, even during periods of increased rainfall and runoff from the crop areas surrounding the lake, as well as transportation of particulate material by the two main tributaries of the lake (the Pardo River and the Peixe River), the lake tends to homogenize the content of TSS due to its large size and average depth of 30 m when the rain decreases in intensity in the region or is attenuated due to the change of season. This allows for time lapses to balance TSS within the water column. The second aspect was a gradual increase during the first two observed periods in the series, reaching an increase of 0.59 mgL⁻¹ (from May 2000 to October 2009). However, the third period within the series shows an increase of 3.92 mgL⁻¹ compared to the first average value of the time series. This period mainly shows that the rains generated by the “La Niña” phenomenon between 2010 and 2011 significantly affected the TSS content within the lake. The value increased slightly (0.13 mgL⁻¹) in the range of 2015-2020 compared to the previous period (2010-2015).

The BFAST algorithm demonstrated its advantages over traditional methods for decomposing time series such as STL. BFAST not only effectively extracted the trend, seasonality, and random components; but it also allowed us to find the inflection points that affect the amount of TSS within the lake, and it was also possible to associate these inflection points with external natural factors and those caused by humans.

4. CONCLUSIONS

This article proposes a novel approach when analyzing the dynamics of a time series including reflectance images produced by the MODIS sensor using the BFAST algorithm. The R function proved to have advantages over other time series decomposition techniques. The main utility applied in this study was to identify variation points within the trend. It was also possible, based on the results, to associate interval oscillation with aspects such as lake construction, increased rainfall, and weather events such as “la niña” affecting the TSS behavior. Similarly, seasonal analysis found two intervals in which the number of suspended

solids in water is increased, the first one is related to rains that produce sedimentation in tributary rivers (Pardo River and do Peixe River) and the flow of particulate matter from crop areas surrounding the lake; the second one is associated with algae growth after lake fertilization produced by rains.

Moreover, it was also possible to develop a model based on the spectral response of band 1 (645 nm) of MODIS MOD09GA products. This algorithm was useful to retrieve the TSS parameter. The statistical estimators used to validate the model showed a high coefficient of determination ($R^2 = 0.82$) and low errors associated with observations ($RMSE = 2.7 \text{ mgL}^{-1}$).

Finally, the high temporal resolution of the MOD09GA product, was adequate to analyze the time series generated. Similarly, the prior analysis of MOD09GA image information enabled an appropriate planning to define the spatial distribution of sampling points and the dates in which more relevant information could be obtained.

REFERENCES

- [1] M. J. Butt, and M. Nazeer, "Landsat ETM+ Secchi Disc Transparency (SDT) retrievals for Rawal Lake, Pakistan," *ScienceDirect*, vol. 56, no. 7, pp. 1428-1440, Oct. 2015. <https://doi.org/10.1016/j.asr.2015.06.041>
- [2] Z. Cao, H. Duan, L. Feng, R. Ma, and K. Xue, "Climate- and human-induced changes in suspended particulate matter over Lake Hongze on short and long timescales," *Remote Sensing of Environment*, vol. 192, pp. 98-113, Apr. 2017. <https://doi.org/10.1016/j.rse.2017.02.007>
- [3] M. H. Gholizadeh, A. M. Melesse, and L. Reddi, "Comprehensive review on water quality parameters. Estimation using Remote Sensing Techniques," *Sensors*, vol. 16, no. 8, p. 1298, Aug. 2016. <https://doi.org/10.3390/s16081298>
- [4] C. Giardino, M. Pepe, P. A. Brivio, P. Ghezzi, and E. Zilioli, "Detecting chlorophyll, Secchi disk depth and surface temperature in a sub-alpine lake using Landsat imagery," *The Science of the Total Environment*, vol. 268, no. 1-3, pp. 19-29, Mar. 2001. [https://doi.org/10.1016/S0048-9697\(00\)00692-6](https://doi.org/10.1016/S0048-9697(00)00692-6)
- [5] X. Hou, L. Feng, H. Duan, X. Chen, D. Sun, and K. Shi, "Fifteen-year monitoring of the turbidity dynamics in large lakes and reservoirs in the middle and lower basin of the Yangtze River, China," *Remote Sensing of Environment*, vol. 190, pp. 107-121, Mar. 2017. <https://doi.org/10.1016/j.rse.2016.12.006>
- [6] E. M. Ruzycki, R. P. Axler, G. E. Host, J. R. Henneck, and N. R. Will, "Estimating sediment and nutrient loads in four western Lake Superior streams," *Journal of the American Water Resources Association*, vol. 50, no. 5, pp. 1138-1154, Oct. 2014. <https://doi.org/10.1111/jawr.12175>
- [7] J. Hui, L. Yao, and Z. Wen-bin, "Retrieval and Analysis of Total Suspended Solid Concentration by MODIS Terra 500m Imagery during Flood Period in Poyang Lake, China," in *2011 International Conference on Computer Distributed Control and Intelligent Environmental Monitoring*, Changsha, China, 2011, pp. 985-988. <https://doi.org/10.1109/CDCIEM.2011.480>
- [8] M. Wang, S. Son, Y. Zhang, and W. Shi, "Remote sensing of water optical property for China's Inland Lake Taihu using the SWIR Atmospheric correction with 1640 and 2130nm Bands," *IEEE Journal of selected topics in applied earth observations and remote sensing*, vol. 6, no. 6, pp. 2505-2516, Dec. 2013. <https://doi.org/10.1109/JSTARS.2013.2243820>
- [9] Z. Wang, K. Kawamura, Y. Sakuno, X. Fan, Z. Gong, and J. Lim, "Retrieval of chlorophyll-a and total suspended solids using Iterative Stepwise Elimination Partial Least Squares (ISE-PLS) Regression based on field hyperspectral measurements in irrigation ponds in Higashihiroshima, Japan," *Remote Sensing*, vol. 9, no. 3, p. 264, Mar. 2017. <https://doi.org/10.3390/rs9030264>
- [10] G. S. Bilotta et al., "Developing environment-specific water quality guidelines for suspended particulate matter," *Water Res.*, vol. 46, no. 7, pp. 2324-2332, May. 2012. <https://doi.org/10.1016/j.watres.2012.01.055>
- [11] G. Bilotta, and R. Brazier, "Understanding the influence of suspended solids on water quality and aquatic biota," *Water Research*, vol. 42, no. 12, pp. 2849-2861, Jun. 2008. <https://doi.org/10.1016/j.watres.2008.03.018>
- [12] F. L. Hellweger, P. Schlosser, U. Lall, and J. K. Weissel, "Use of satellite imagery for water quality studies in New York Harbor," *Estuar. Coast. Shelf Sci.*, vol. 61, no. 3, pp. 437-448, 2004. <https://doi.org/10.1016/j.ecss.2004.06.019>

- [13] Y. Liu, A. Islam, and J. Gao, "Quantification of shallow water quality parameters by means of remote sensing," *Progress in Physical Geography*, vol. 27, no. 1, pp. 24-43, Mar. 2003. <https://doi.org/10.1191/0309133303pp357ra>
- [14] N. L. Lailia, F. Arafah, A. Jaelani, and A. D. Pamungkas, "Development of water quality parameter retrieval algorithms for estimating total suspended solids and chlorophyll-a concentration using Landsat-8 imagery at Poteran island water," *Remote Sensing and Spatial Information Sciences*, vol. II, no. 2, Mar. 2015. <http://eprints.itn.ac.id/2852/1/isprsannals-II-2-W2-55-2015.pdf>
- [15] Y. Zhang, R. Ma, H. Duan, S. Loisselle, M. Zhang, and J. Xu, "A novel MODIS algorithm to estimate chlorophyll a concentration in eutrophic turbid lakes," *Ecological Indicators*, vol. 69, pp. 138-151, Oct. 2016. <https://doi.org/10.1016/j.ecolind.2016.04.020>
- [16] C. Östlund, P. Flink, N. Strömbeck, D. Pierson, and T. Lindell, "Mapping of the water quality of Lake Erken, Sweden, from Imaging Spectrometry and Landsat Thematic Mapper," *The Science of the Total Environment*, vol. 268, no. 1-3, pp. 139-154, Mar. 2001. [https://doi.org/10.1016/S0048-9697\(00\)00683-5](https://doi.org/10.1016/S0048-9697(00)00683-5)
- [17] P. Dorji, P. Fearn, and M. Broomhall, "A semi-analytic model for estimating Total Suspended Sediment concentration in turbid coastal waters of Northern Western Australia Using MODIS-Aqua 250m Data," *Remote Sensing*, vol. 8, no. 7, p. 556, Jun. 2016. <https://doi.org/10.3390/rs8070556>
- [18] D. Doxaran, J. M. Froidefond, P. Castaing, and M. Babin, "Dynamics of the turbidity maximum zone in a macrotidal estuary (the Gironde, France): Observations from field and MODIS satellite data," *Estuarine, Coastal and Shelf Science*, vol. 81, no.3, pp. 321-332, Feb. 2009. <https://doi.org/10.1016/j.ecss.2008.11.013>
- [19] A. R. M. Amin, K. Abdullah, H. S. Lim, M. F. Embong, F. Ahmad, and R. Yaacob, "Development of regional TSS algorithm over Penang using Modis Terra (250 M) surface reflectance product," *Ekológia(Bratislava)*, vol. 35, no. 3, pp. 289-294, Sep. 2016. <https://doi.org/10.1515/eko-2016-0023>
- [20] C. Petus, G. Chust, F. Gohin, D. Doxaran, J. M. Froidefond, and Y. Sagarminaga, "Estimating turbidity and total suspended matter in the adour river plume (South Bay of Biscay) using MODIS 250 m imagery," *Continental Shelf Research*, vol. 30, no. 5, pp. 379-392, Mar. 2010. <https://doi.org/10.1016/j.csr.2009.12.007>
- [21] E. Kaba, W. Philpot, and T. Steenhuis, T, "Evaluating suitability of MODIS-Terra images for reproducing historic sediment concentrations in water bodies: Lake Tana, Ethiopia," *International Journal of Applied Earth Observation and Geoinformation*, vol. 26, pp. 286-297, Feb. 2014. <https://doi.org/10.1016/j.jag.2013.08.001>
- [22] N. Bi, Z. Yang, H. Wang, D. Fan, X. Sun, and K. Lei, "Seasonal variation of suspended-sediment transport through the southern Bohai Strait," *Estuarine Coastal and Shelf Science*, vol. 93, no. 3, pp. 239-247, Jul. 2011. <https://doi.org/10.1016/j.ecss.2011.03.007>
- [23] Z. Chen, C. Hu, and F. Muller-Karger, "Monitoring turbidity in Tampa Bay using MODIS/Aqua 250-m imagery," *Remote Sensing of Environment*, vol. 109, no. 2, pp. 207-220, Jul. 2007. <https://doi.org/10.1016/j.rse.2006.12.019>
- [24] J. E. Min, J. H. Ryu, S. Lee, and S. H. Son, "Monitoring of suspended sediment variation using Landsat and MODIS in the Saemangeum coastal area of Korea," *Marine Pollution Bulletin*, vol. 64, no. 2, pp. 382-390, Feb. 2012. <https://doi.org/10.1016/j.marpolbul.2011.10.025>
- [25] M. Hasan, and L. Benninger, "Resiliency of the western Chesapeake Bay to total suspended solid concentrations following storms and accounting for land-cover," *Estuarine, Coastal and Shelf Science*, vol. 191, pp. 136-149, May. 2017. <https://doi.org/10.1016/j.ecss.2017.04.002>

- [26] E. K. Ayana, A. W. Worqlul, and T. S. Steenhuis, "Evaluation of stream water quality data generated from MODIS images in modeling total suspended solid emission to a freshwater lake," *Science of the total Environment*, vol. 523, pp. 170-177, Aug. 2015. <https://doi.org/10.1016/j.scitotenv.2015.03.132>
- [27] E. M. L. de Moraes Novo, C. C. Faria Barbosa, J. M. Melack, R. Moraes de Freitas, F. Titonelli, and Y. Shimabukuro, "Comparing MODIS and etm+ image data for inland water studies: spatial resolution constraints," *Revista Brasileira de Cartografia*, vol. 58, no. 2 pp. 109-118, Aug. 2006. <https://scholar.archive.org/work/caab3zgp1ndzzlqy7py6osl7ju/access/wayback/http://www.seer.ufu.br/index.php/revistabrasileiracartografia/article/download/44916/23926/>
- [28] J. Knight, and M. L. Voth, "Application of MODIS imagery for intra-annual water clarity assessment of Minnesota Lakes," *Journal of remote sensing of environment*, vol. 4, no. 7, pp. 2181-2198, Jul. 2012. <https://doi.org/10.3390/rs4072181>
- [29] I. M. McCullough, C. S. Loftin, and S. A. Sader, "High-frequency remote monitoring of large lakes with MODIS 500m imagery," *Remote Sens. Environ.*, vol. 124, pp. 234-241, Sep. 2012. <https://doi.org/10.1016/j.rse.2012.05.018>
- [30] R. Moncayo, "Mapeo de la dinámica regional de la transparencia en aguas continentales usando productos de reflectancia MOD09GA," *Entramado*, vol. 13, no. 2, pp. 270-276, jun. 2017. <https://doi.org/10.18041/entramado.2017v13n2.26233>
- [31] E. E. Souza Filho, "The Porto Primavera dam and the fluvial transport on the Porto são José section, Parana river" *Mercator*, vol. 15, no. 4, pp. 65-81, 2016. <https://doi.org/10.4215/RM2016.1504.0005>
- [32] J. Dias, "A construção da paisagem na raia divisória são paulo-paraná-mato grosso do sul: um estudo por teledeteção" (Tese de Doutorado), Departamento de Geografia, Universidade Estadual Paulista – UNESP - Presidente Prudente, Brasil, 2003. <https://repositorio.unesp.br/server/api/core/bitstreams/05b51ab9-cb4c-48c1-80c7-f3feb70b1740/content>
- [33] Z. Cao *et al.*, "MODIS observations reveal decrease in lake suspended particulate matter across China over the past two decades," *Remote Sens. Environ.*, vol. 295, no. 113724, p. 113724, Sep. 2023. <https://doi.org/10.1016/j.rse.2023.113724>
- [33] Z. Cao *et al.*, "MODIS observations reveal decrease in lake suspended particulate matter across China over the past two decades," *Remote Sens. Environ.*, vol. 295, no. 113724, p. 113724, Sep. 2023. <https://doi.org/10.1016/j.rse.2023.113724>
- [34] E. Ghaderpour, and T. Vujadinovic, "Change Detection within Remotely Sensed Satellite Image Time Series via Spectral Analysis," *Remote Sensing*, vol. 12, no. 23, p. 4001, Dec. 2020. <https://doi.org/10.3390/rs12234001>
- [35] D. Masiliūnas, T. Nandin-Erdene, M. Herold, and J. Verbesselt, "BFAST Lite: A lightweight break detection method for time series analysis," *Remote Sens. (Basel)*, vol. 13, no. 16, p. 3308, Aug. 2021. <https://doi.org/10.3390/rs13163308>
- [36] C. A. Tassinari, S. H. Bonilla, F. Agostinho, C. M. V. B. Almeida, and B. F. Giannetti, "Evaluation of two hydropower plants in Brazil: using energy for exploring regional possibilities," *J. Clean. Prod.*, vol. 122, pp. 78-86, 2016. <https://doi.org/10.1016/j.jclepro.2016.01.077>
- [37] L. Sabo Boschi, M. L. B. T. Galo, L. H. S. Rotta, and F. S. Y. Watanabe, "Mapeamento do biovolume de plantas aquáticas submersas a partir de dados hidroacústicos e imagem multiespectral de alta resolução," *Planta Daninha*, vol. 30, no. 3, pp. 525-539, Sep. 2012. <https://www.scielo.br/j/pd/a/3gX3NnzbVjw3N7LZMCRvvpG/#>

- [38] R. L. Miller, B. A. Mckee, “Using MODIS Terra 250 m imagery to map concentrations of total suspended matter in coastal waters,” *Remote Sensing of Environment*, vol. 93, no. 1-3, pp. 259-266, Oct. 2004. <https://doi.org/10.1016/j.rse.2004.07.012>
- [39] R. G. Wetzel, and G. E. Likens, *Limnological analyses*, New York, USA: Springer, 1991.
- [40] E. F. Vermote, N. Z. El Saleous, and C. O. Justice, “Atmospheric correction of MODIS data in the visible to middle infrared: first results,” *Remote Sensing of Environment*, vol. 83, no. 1-2, pp. 97-111, Nov. 2002. [https://doi.org/10.1016/S0034-4257\(02\)00089-5](https://doi.org/10.1016/S0034-4257(02)00089-5)
- [41] Y. Zhang et al., “Temporal and spatial variability of chlorophyll a concentration in Lake Taihu using MODIS time-series data,” *Hydrobiologia*, vol. 661, no. 1, pp. 235–250, Feb. 2011. <https://doi.org/10.1007/s10750-010-0528-9>
- [42] L. Zhu, S. Wang, Y. Zhou and F. Yan, “Estimation of Suspended Sediment Concentration Changes in Taihu Lake Based on Multi-temporal MODIS Image Data,” in *2006 IEEE International Symposium on Geoscience and Remote Sensing*, Denver, CO, USA, 2006, pp. 3023-3026. <https://doi.org/10.1109/IGARSS.2006.776>
- [43] B. F. Rudorff, “aplicações de MODIS em estudos epidemiológicos” in *Sensor Modis e Suas Aplicações Ambientas no Brasil*, Editora Parêntese, 2007, pp. 207-209. https://books.google.com/books?id=4MxI4hZQeOEC&printsec=frontcover&dq=inauthor:%22BERNARDO+F.+T.+RUDORFF+Rudorff%22&hl=es&newbks=1&newbks_redir=1&sa=X&ved=2ahUKEwiiyKSKipiIAxWNSjABHUtVDY8Q6AF6BAgHEAI
- [44] D. C. Hatchell, *Analytical Spectral Devices, Technical Guide*, New York – USA, (1999). Accessed: Jan. 5, 2023. [Online]. Available: <https://www.gep.uchile.cl/Biblioteca/radiometr%C3%ADa%20de%20campo/TechGuide.pdf>
- [45] C. D. Mobley, “Estimation of the remote-sensing reflectance from above-surface measurements,” *Appl. Opt.*, vol. 38, no. 36, p. 7442, Dec. 1999. <https://doi.org/10.1364/ao.38.007442>
- [46] S. Chen, L. Han, X. Chen, D. Li, and Y. Li, “Estimating wide range Total Suspended Solids concentrations from MODIS 250-m imageries: An improved method,” *ISPRS Journal of Photogrammetry and Remote Sensing*, vol. 99, pp. 58-69, Jan. 2015. <https://doi.org/10.1016/j.isprsjprs.2014.10.006>
- [47] G. Dall'olmo, A. A. Gitelson, D. C. Rundquist, B. Leavitt, T. Barrow, and J. C. Holz, “Assessing the potential of Sea WIFS and MODIS for estimating chlorophyll concentration in turbid productive waters using red near-infrared bands,” *Remote Sensing of Environment*, vol. 96, no. 2, pp. 176-187, May. 2005. <https://doi.org/10.1016/j.rse.2005.02.007>
- [48] MODIS ProtoFlight Model (PFM) *Relative Spectral Response (RSR)*, *Science Team - MODIS web – NASA*, 1999, Available at: ftp://mcst.ssaihq.com/pub/permanent/MCST/PFM_L1B_LUT_4-30-99/L1B_RSR_LUT/
- [49] M. Matthews, “Current review of empirical procedures of remote sensing in inland and near-coastal transitional waters,” *International Journal of Remote Sensing*, vol. 32, pp. 6855-6899, Aug. 2011. <http://dx.doi.org/10.1080/01431161.2010.512947>
- [50] J. J. Wang, and X. X. Lu, “Estimation of suspended sediment concentrations using Terra MODIS: an example from the Lower Yangtze River, China,” *Science of The Total Environment*, vol. 408, no. 5, pp. 1131–1138, Feb. 2010. <https://doi.org/10.1016/j.scitotenv.2009.11.057>
- [51] K. Shi et al., “Long-term remote monitoring of total suspended matter concentration in Lake Taihu using 250m MODIS-Aqua data,” *Remote Sens. Environ.*, vol. 164, pp. 43–56, Jul. 2015. <https://doi.org/10.1016/j.rse.2015.02.029>

- [52] A. G. Dekker, R. J. Vos, and S. W. M. Peters, "Analytical algorithms for lake water TSM estimation for retrospective analyses of TM and SPOT sensor data," *Int. J. Remote Sens.*, vol. 23, no. 1, pp. 15–35, 2002. <https://doi.org/10.1080/01431160010006917>
- [53] E. Park, and E. M. Latrubesse, "Modeling suspended sediment distribution patterns of the Amazon River using MODIS data," *Remote Sens. Environ.*, vol. 147, pp. 232–242, May. 2014. <https://doi.org/10.1016/j.rse.2014.03.013>
- [54] V. Rodríguez-Guzmán, and F. Gilbes-Santaella, "Using MODIS 250 m imagery to estimate total suspended sediment in a tropical open bay," *Int. J. Syst. Appl. Eng. Dev.*, vol. 3, no. 1, pp. 36–44, 2009. https://www.uprm.edu/gerslab/wp-content/uploads/sites/214/2023/07/rodriguez_gilbes_09b.pdf
- [55] B. Demir, F. Bolovo, and L. Bruzzone, "Classification of time series of multispectral images with limited training data," *IEEE Transactions on Image Processing*, vol. 22, no. 8, pp. 3219–3233, Aug. 2013. <https://doi.org/10.1109/TIP.2013.2259838>
- [56] J. Verbesselt, R. Hyndman, G. Newnham, and D. Culvenor, "Detecting trend and seasonal changes in satellite image time series," *Remote Sensing of Environment*, vol. 114, no. 1, pp. 106–115, Jan. 2010. <https://doi.org/10.1016/j.rse.2009.08.014>
- [57] M. Lu, E. Pebesma, A. Sánchez, and J. Verbesselt, "Spatio-temporal change detection from multidimensional arrays: Detecting deforestation from MODIS time series," *ISPRS Journal of Photogrammetry and Remote Sensing*, vol. 117, pp. 227–236, 2016. <https://doi.org/10.1016/j.isprsjprs.2016.03.007>
- [58] J. Lambert, A. Jacquin, J. Denux, and V. Chéret, "Comparison of two remote sensing time series analysis methods for monitoring forest decline," *Multi temp. 6th International Workshop on the Analysis of Multi-temporal Remote Sensing Images (Multi-temp)*, Trento, Italy, 2009, pp. 93–96. <https://doi.org/10.1016/j.isprsjprs.2016.03.007>
- [59] P. A. Permatasari, A. Fatikhunnada, Liyantono, Y. Setiawan, Syartinilia, and A. Nurdiana, "Analysis of agricultural land use changes in jombang regency, east java, Indonesia using BFAST method," *Procedia Environ. Sci.*, vol. 33, pp. 27–35, 2016. <https://doi.org/10.1016/j.proenv.2016.03.053>
- [60] L. Feng, C. Hu, X. Han, X. Chen, and L. Qi, "Long-Term Distribution Patterns of Chlorophyll-a Concentration in China's Largest Freshwater Lake: MERIS Full-Resolution Observations with a Practical Approach," *Remote sensing*, vol. 7, no. 1, pp. 275–299, Dec. 2015. <https://doi.org/10.3390/rs70100275>
- [61] A. A. Gitelson, D. Gurlin, W. J. Moses, and T. Barrow, "A bio-optical algorithm for the remote estimation of the chlorophyll-*a* concentration in case 2 waters," *Environ. Res. Lett.*, vol. 4, no. 4, p. 045003, 2009. <https://doi.org/10.1088/1748-9326/4/4/045003>
- [62] C. Le et al., "Towards a long-term chlorophyll-a data record in a turbid estuary using MODIS observations," *Prog. Oceanogr.*, vol. 109, pp. 90–103, Feb. 2013. <https://doi.org/10.1016/j.pocean.2012.10.002>
- [63] Y. Zhang, S. Lin, J. Liu, X. Qian, and Y. Ge, "Time-series MODIS image-based retrieval and distribution analysis of total suspended matter concentrations in Lake Taihu (China)," *Int. J. Environ. Res. Public Health*, vol. 7, no. 9, pp. 3545–3560, 2010. <https://doi.org/10.3390/ijerph7093545>
- [64] J. Zhao et al., "Remote sensing evaluation of total suspended solids dynamic with Markov model: A case study of inland reservoir across administrative boundary in South China," *Sensors (Basel)*, vol. 20, no. 23, p. 6911, Dec. 2020. <https://doi.org/10.3390/s20236911>

- [65] Y. Yang, and Y. Wang, “Using the BFAST Algorithm and Multitemporal AIRS Data to Investigate Variation of Atmospheric Methane Concentration over Zoige Wetland of China,” *Remote Sensing*, vol. 12, no. 19, pp. 1-17, 2020. <https://doi.org/10.3390/rs12193199>
- [66] J. C. Stevaux, D. P. Martins, and M. Meurer, “Changes in a large regulated tropical river: The Paraná River downstream from the Porto Primavera Dam, Brazil,” *Geomorphology (Amst.)*, vol. 113, no. 3–4, pp. 230–238, Dec. 2009. <https://doi.org/10.1016/j.geomorph.2009.03.015>
- [67] E. Ciancia et al., “Modeling and multi-temporal characterization of total suspended matter by the combined use of sentinel 2-MSI and Landsat 8-OLI data: The Pertusillo Lake case study (Italy),” *Remote Sens. (Basel)*, vol. 12, no. 13, p. 2147, Jul. 2020. <https://doi.org/10.3390/rs12132147>
- [68] G. B. Chelotti, J. M. Martinez, H. L. Roig, and D. Olivetti, “Space-Temporal analysis of suspended sediment in low concentration reservoir by remote sensing,” *RBRH*, vol. 24, p. e17, 2019. <https://www.scielo.br/j/rbrh/a/rcbdD6j8VZVD5pVBqRtDZgR/?lang=en>
- [69] Z. Tan, Z. Cao, M. Shen, J. Chen, Q. Song, and H. Duan, “Remote estimation of water clarity and suspended particulate matter in Qinghai Lake from 2001 to 2020 using MODIS images,” *Remote Sens. (Basel)*, vol. 14, no. 13, p. 3094, 2022. <https://doi.org/10.3390/rs14133094>

Notes

5. ACKNOWLEDGEMENTS

:

The authors express gratitude to the Universidade Estadual Paulista “Júlio de Mesquita Filho” and to the Master’s degree program in Cartography, to sponsor this research project with both infrastructure and financial resources. Also, we thank to the MODIS project which allowed me to download gratuitously the MOD09GA surface reflectance data and to the FEPAP for its financial support in the fieldworks I carried out. Finally, we are grateful with the UNESP and the AIUP for the doctoral scholarship and CESMAG University for its support given in editing and presenting this manuscript.

CONFLICT OF INTERESTS

:

The authors declare that they have no conflict of interest.

AUTHORSHIP CONTRIBUTION

:

- *Ricardo Javier Moncayo Eraso*: Conception, Data Acquisition, Data interpretation.

- *Francisco Javier Eraso-Checa*: Data analysis, Paper writing and review.

Additional information

How to cite / Cómo citar: R. J. Moncayo Eraso, and F. Eraso-Checa, “Trend Analysis of Total Suspended Solids in Inland Waters Using the BFAST Algorithm on MOD09GA Products in Porto Primavera Reservoir – Brazil,” *TecnoLógicas*, vol. 27, no. 60, e2985, 2024. <https://doi.org/10.22430/22565337.2985>

Alternative link

<https://revistas.itm.edu.co/index.php/tecnologicas/issue/view/138> (html)



Available in:

<https://www.redalyc.org/articulo.oa?id=344277854013>

How to cite

Complete issue

More information about this article

Journal's webpage in redalyc.org

Scientific Information System Redalyc
Network of Scientific Journals from Latin America and the
Caribbean, Spain and Portugal
Project academic non-profit, developed under the open
access initiative

Ricardo Javier Moncayo Eraso, Francisco Eraso-Checa

**Trend Analysis of Total Suspended Solids in Inland Waters
Using the BFAST Algorithm on MOD09GA Products in
Porto Primavera Reservoir – Brazil**

**Análisis de tendencia del total de sólidos en suspensión
en aguas interiores aplicando el algoritmo BFAST a
productos MOD09GA en el embalse de Porto Primavera-
Brasil**

Tecnológicas

vol. 27, no. 60, p. 1 - 19, 2024

Instituto Tecnológico Metropolitano, Colombia

tecnologicas@itm.edu.co

ISSN: 0123-7799

ISSN-E: 2256-5337

DOI: <https://doi.org/10.22430/22565337.2985>



CC BY-NC-SA 4.0 LEGAL CODE

**Licencia Creative Commons Atribución-NoComercial-
CompartirIgual 4.0 Internacional.**